Supporting information for "Solar/Radiative Cooling Dual-Regulation Smart Window Based on Shape-morphing Kirigami Structures"

Shancheng Wang,[a,b‡] Yuting Dong, [b,‡] Yanbin Li,[c,‡] Keunhyuk Ryu,[b] Zhili Dong,[b] Jian Chen,[d] Zhendong Dai,[d] Yujie Ke,[e,*] Jie Yin,[c,*] and Yi Long[a,f,*]

[a]Department of Electrical Engineering, The Chinese University of Hong Kong, Shatin, New Territories, Hong Kong SAR, China

[b]School of Materials Science and Engineering, Nanyang Technological University, 639798 Singapore

[c]Department of Mechanical and Aerospace Engineering, North Carolina State University, Raleigh, North Carolina 27695, United States

[d]Jiangsu Provincial Key Laboratory of Bionic Functional Materials, College of Mechanical and Electrical Engineering, Nanjing University of Aeronautics and Astronautics, Nanjing 210016, China

[e]Institute of Materials Research and Engineering (IMRE), Agency for Science, Technology and Research (A*STAR), 2 Fusionopolis Way, Innovis #08-03, Singapore 138634, Republic of Singapore

[f]Institute of Environment, Energy and Sustainability (IEES), The Chinese University of Hong Kong, Shatin, New Territories, Hong Kong SAR, China

‡These authors contributed equally to this work.

Email: yilong@cuhk.edu.hk; jyin8@ncsu.edu; yujie_ke@imre.a-star.edu.sg

Experiment and method

Materials

N-isopropylacrylamide (NIPAm, 98%, Wako Pure Chemical Industries Ltd), ammonium persulfate (APS, 98%, Sigma-Aldrich), N,N,N',N'-tetramethylethylenediamine (TEMED, 99%, Sigma-Aldrich), acrylamide (AAm, 98%, Sigma-Aldrich), N,N-methylenebis(acrylamide) (Bis, 99%, Sigma-Aldrich), 2-hydroxy-4'-(2-hydroxyethoxy)-2-methylpropiophenone, (98%, Sigma-Aldrich), benzophenone (99%, Sigma-Aldrich), methanol (99.8%, Sigma-Aldrich), acetone (99.8%, Fisher Chemical), glycerol (99.5%, Sigma-Aldrich), polyvinylpyrrolidone (PVP, average Mw≈40000, Sigma-Aldrich), sodium chloride (NaCl, 99%, Sigma-Aldrich), silver nitrate (99%, Sigma-Aldrich), ethanol (99.8%, Fisher Chemical) and SYLGARD™ 184 silicone elastomer kit of polydimethylsiloxane (PDMS, Dow Corning) were used without further purification. Deionized water (DI water) was used throughout the experiments.

Preparation of physically crosslinked smart PNIPAm hydrogel

The preparation of physically crosslinked PNIPAm follows the method reported in the literature.[1] 2.2625 g (0.02 mol) of NIPAm was dissolved in 23 ml of DI water at 25 °C by stirring in an atmosphere of argon to remove solved oxygen. Two aqueous solutions were prepared by dissolving 13.69 mg (0.06 mmol) of APS (initiator) in 1 ml of DI water and 27 µl (0.18 mmol) of TEMED (accelerator) with 1 ml of DI water, followed by mixing with the NIPAm solution at 300 rpm for 30 min to form 25 ml of homogenous solution. Then the solution was left for reaction for 24 h at room temperature. Finally, acetone was added to the solution to precipitate PNIPAm, and the obtained PNIPAm was dried in a vacuum oven at 60 °C.

Preparation of monomer ink for lamination

Monomer ink with 5wt%, 10wt%, 15wt%, and 20wt% PNIPAm concentrations was prepared. Respectively, 0.5 g, 1 g, 1.5 g and 2 g of the pure PNIPAm hydrogel was dissolved in 10 ml DI of water, followed by adding 2 g of AAm and stirring for 30 min. Then, 0.02 g of Bis and 0.1 g of 2-hydroxy-4'-(2-hydroxyethoxy)-2-methylpropiophenone (light initiator) was added and the mixture was stirred well. The monomer ink was prepared for lamination in later step.

Synthesis of AgNWs

The AgNWs were prepared according to the literature.[2] 1.76 g of polyvinylpyrrolidone (PVP) was added to 57 ml of glycerol. The mixture was stirred at 500 rpm for 2 h at 110 °C to form a homogenous solution and was then cooled down to room temperature. Next, 0.474 g of silver nitrate was added to the solution followed by a NaCl solution prepared by dissolving 17.7 mg of NaCl in 0.15 ml of DI water and 3 ml of glycerol. Subsequently, the mixture was heated to 210 °C from room temperature within 30 min under 200 rpm stirring, and heating was stopped when the temperature reached 210 °C. When the mixture cooled down to 100 °C, 60 ml of DI water was added, followed by subsequent cooling to room temperature. The obtained solution was kept undisturbed for one week before the collection of the sediment at the flask bottom. The obtained AgNWs were washed with ethanol thoroughly by centrifuging at 5000 rpm 3 times.

Preparation of PDMS film for the PDMS-composite hydrogel-PDMS sandwich structure

Firstly, the precursor and curing agent of PDMS gel were well mixed at a weight ratio of 10:1, followed by vacuum degassing to remove the bubbles. 2.5 g of the mixture was loaded on a plastic petri dish cover (d=9.5 cm) and spin-coated at 1000 rpm for 30 s. The PDMS was then cured in an oven at 60 °C for ~2 h. The obtained thin PDMS films were cut into the size of 5×5 cm for the subsequent lamination process.

Lamination of the PDMS-composite hydrogel-PDMS sandwich structure

There were three steps for the lamination process, namely (1) pre-treatment of PDMS film, (2) sealing, and (3) crosslinking. (1) For the pre-treatment step, two pieces of PDMS thin films were immersed in a benzophenone solution (20wt% in acetone) to facilitate chemical bonds between PDMS and PNIPAm for 15 min. Then, the thin films were rinsed with methanol and dried in a vacuum desiccator. (2) For the subsequent sealing process, one piece of benzophenone immersed PDMS film was transferred to a glass substrate and covered by a mould with a 5 cm × 5 cm × 1 mm square hole. The monomer ink was then poured into the hole of the mould. And another benzophenone immersed PDMS film was placed onto the mould to cover the uncrosslinked monomer ink. The side of structure was then sealed with epoxy. (3) Finally, for the crosslinking step, the sealed sandwich structure was exposed under 365 nm UV for 5 min for the hydrogel to fully crosslink.

Spin coating of AgNWs

Prepared AgNWs were dispersed in ethanol and ultrasonicated to form a suspension of ~5 mg/ml. The fabricated sandwich structure was pre-strained to 40% and treated by O_2 plasma for 1 min. Then, 0.75 ml of the AgNWs suspension was spin-coated at 1000 rpm for 30 s. The coating process was conducted 1, 5, 10, and 15 times for the samples with 1, 5, 10, and 15 layers of AgNWs.

Preparation of PDMS films for kirigami structure

2.5 g of PDMS precursor and 0.25 g of PDMS curing agent were mixed with 2.75 g of hexane. The mixture was transferred to a plastic petri dish (d=9.5 cm). The hexane was removed by ~1 h evaporation at room temperature in a fume hood. Then, the stiff mixture was cured in an oven under 60 °C for ~2 h to make thick PDMS films.

Preparation of reconfigurable kirigami structure

The designed kirigami patterns were printed on paper and cut manually to get the paper kirigami structures. The PDMS kirigami structures were cut manually using the printed kirigami pattern as a template.

Morphological characterization of smart hydrogel and the AgNWs

The SEM images of smart hydrogel and AgNWs were taken with SEM Supra 55 (Carl Zeiss). To obtain the microstructure of hydrogels below and above LCST (20 °C), the two samples of smart hydrogel were placed at 15 and 45 °C separately for 1 h. Then the two samples were immediately submerged in liquid nitrogen until fully frozen. Due to the extremely low temperature of liquid nitrogen, the microstructures of the hydrogel at different temperatures were preserved.[3] The frozen hydrogels were placed into a freeze-dryer for the freeze-drying process for 72 h. The freeze-dried aerogels were subsequently used to take the SEM images.

The AgNWs were coated onto PDMS substrate and the SEM images for the released and stretched states were captured.

Rheological characterization of smart hydrogel samples

The rheological properties of the composite hydrogel inks with 5%, 10%, 15% and 20% PNIPAm concentration were measured by Anton Paar MCR 702e rheometer with a cone and plate geometry at a reference temperature of 15 °C. Hydrogel with a thickness of 0.5 mm and diameter of 15 mm was prepared. The storage modulus (G') and loss modulus (G'') were measured at a constant oscillatory shear strain of 0.5% with angular frequency ranging from 100 rad/s to 0.1 rad/s. The viscosity was measured with shear rates ranging from 0.01 to 100 s^{-1}.

Optical characterization of smart hydrogel, AgNWs, kirigami structures, and smart window

A UV-Vis spectrometer system (AvaSpec-ULS2048L StarLine Versatile Fiber-optic Spectrometer and AvaSpec-NIR256-2.5-HSC-EVO, Avantes) with a heating/cooling stage (PE120, Linkam) equipped was employed to collect the UV-Vis-NIR transmittance and reflectance spectra. The luminous transmittance (T_{lum}, 360-780 nm), IR transmittance ($T_{IR,}$ 780-2500 nm), and solar transmittance (T_{sol}, 250-2500 nm) were calculated by Equation 1:[4]

$$T_{lum/IR/sol} = \int \varphi_{lum/sol} T(\lambda) d\lambda \Big/ \int \varphi_{lum/sol} d\lambda \quad (1)$$

In this formula $T(\lambda)$ is spectral transmittance, $\psi_{lum}(\lambda)$ is the standard luminous efficiency function of photopic vision in the wavelength range of 360–780 nm[5]. On the other hand, $\psi_{sol}(\lambda)$ is the solar irradiance spectrum for air mass 1.5 (corresponding to the sun standing 37° above the horizon with 1.5-atmosphere thickness, which corresponds to a solar zenith angle of 48.2°)[6]. The solar modulation ability ΔT_{sol} was calculated with Equation 2:

$$\Delta T_{NIR/sol} = T_{NIR/sol,\,20℃} - T_{NIR/sol,90℃} \quad (2)$$

The reflectance R_{lum} and R_{sol} were calculated using Equation 3:

$$R_{lum/sol} = \int \varphi_{lum/sol} R(\lambda) d\lambda \Big/ \int \varphi_{lum/sol} d\lambda \quad (3)$$

Where $R(\lambda)$ is the spectral reflectance (360-780 nm for R_{lum} and 250-2500 nm for R_{sol}). $\psi_{lum}(\lambda)$ is the standard luminous efficiency function of photopic vision for the wavelength of 360–780 nm while $\psi_{sol}(\lambda)$ is the solar irradiance spectra for air mass 1.5, respectively.

Emissivity measurement of AgNWs and smart window

The emissivity curve was plotted according to Kirchhoff's law of thermal radiation: $\varepsilon(\lambda) = A(\lambda) = 1\text{-}T(\lambda)\text{-}R(\lambda)$.[7] $R(\lambda)$ and $T(\lambda)$ are the spectral reflectance and the spectral transmittance that was measured by FTIR spectrometer (Perkin Elmer Frontier) with an integration sphere attached. The integrated broadband emissivity were calculated with Equation 4:[7]

$$\varepsilon_{Broadband} = \frac{\int_{2.5\,\mu m}^{20\,\mu m} I_{BB}(T,\lambda)\varepsilon(T,\lambda)\,d\lambda}{\int_{2.5\,\mu m}^{20\,\mu m} I_{BB}(T,\lambda)d\lambda} \quad (4)$$

$I_{BB}(T, \lambda)$ is the spectral intensity emitted by a blackbody at temperature T and $\varepsilon(T, \lambda)$ is the surface's spectral hemispherical thermal emittance for the wavelength of 2.5-20 μm.

Mechanical characterization of the smart hydrogel and kirigami samples

The mechanical properties of smart hydrogel and paper kirigami were tested by Instron 5567 mechanical tester with tensile extension mode. Rectangular hydrogel samples with a thickness of 0.5 mm were prepared for the mechanical test. For PDMS kirigami samples, MTS Mechanical Tester Model 42 was used to measure the mechanical properties.

Numerical performance evaluation of the reconfigurable kirigami structure

Two performance indices namely length ratio and covering ratio were defined to quantitatively evaluate the performance of reconfigurable kirigami designs with different asymmetric ratios. The length ratio is defined as the ratio of the lengths of the two sides of the opening labelled as L_1 and L_2, which characterizes the degree of asymmetry for the stretched kirigami structure. The covering ratio is defined as the ratio of the exposed area (A_1) to the total area (A_2) of the out-of-plane kirigami, reflecting the ability of the kirigami structure to expose underlying layers upon stretching.

Mechanical simulation of the reconfigurable kirigami structure

The mechanical simulation of the kirigami structure was conducted with commercial FEM software ABAQUS. Three 5×5 structures are simulated with the asymmetric ratio as 1, 1.5, 3, 5, and 10 separately. The cut widths of all three structures were set as 2 mm and the cut corner was set as a circle-shape with a radius of 1.25 mm to reduce stress concentration. All three different structures were simulated as a three-dimensional problem. Given the experimentally fabricated PDMS (10:1) material, the neo-Hookean energy model was used here with shear modulus as 2 MPa and Poisson's ratio as 0.495 to approximate the incompressibility of hyper-elastic PDMS materials. The C3D8R element type was utilized for mesh. For loading conditions, the top cross-section of the model was totally constrained and only the bottom surface was uniaxially stretched.

Durability measurement of the smart window

The durability measurements with different environmental temperatures were conducted with laminated smart hydrogel and conventional PNIPAm hydrogel. The measurements were conducted with two environment setups: room temperature (25 °C, 10%RH) and high temperature (60 °C, 10%RH). The transmittance at 650 nm at 15 and 45 °C for all samples was measured and the ΔT_{650nm} was calculated. The samples were considered as failed when their ΔT_{650nm} reduced to 0 and the exposure times were recorded as the lifetimes of the samples.

Cycle stability measurement of the smart window

The cycle stability of the smart window was evaluated by measuring its T_{650nm} at 15 and 45 °C after repeating heating/cooling cycles. T_{650nm} at different temperatures were recorded for the original state and every 5 cycles until 125 heating/cooling cycles.

Energy-saving performance simulation for the smart window and literature-reported cases

EnergyPlus was used in the energy consumption simulation. In this simulation, a building model with the dimensions of 8 m in length, 6 m in width, and 2.7 m in height was used. The floor area was 48 m^2 and the total external wall surface area of the building was 75.6 m^2. Four windows with the dimension of 3 m in width and 2 m in height were installed in the four orientations to avoid the impact of orientation. The window covered 31.7% of the total wall surface area. The structure of the model house is shown in figure S20. Hourly weather data for a Typical Meteorological Year (TMY) was employed as the external boundary conditions.[8] In this simulation, the energy usage based on the unit of MJ m^{-2} was calculated based on the floor area.

For the global average energy saving performance comparison, clear glass, durable solar/RC dual-control smart window, RCRT smart window,[9] and STR smart window[10] were used for this simulation. The optical data for clear glass and the smart window are listed in table S3 while the optical data for the rest were obtained from the respective literature. The energy savings of all samples were calculated with the climate data of Singapore; Hong Kong SAR, China; Melbourne, VIC, Australia; Paris, France; London, UK; and Juneau, AK, U.S. (figure S22). The energy-saving data were then averaged to obtain the global average energy-saving performance of different samples.

For the 24-hour room temperature simulation, the clear glass, conventional PNIPAm hydrogel, commercial low-E glass, and durable solar/RC dual-control smart window were employed with their optical data listed in table S3. In this simulation, the HVAC system was switched off. Climate data from Singapore; Hong Kong SAR, China; Paris, France; and Juneau, AK, U.S. were used in this simulation. The climate data for 15th January was used in the winter room temperature simulation, and the climate data for 15th July was used in the summer room temperature simulation. It is worth mentioning that due to its tropical climate, there is no winter season in Singapore. Therefore, the room temperature curves in January and July are similar for Singapore.

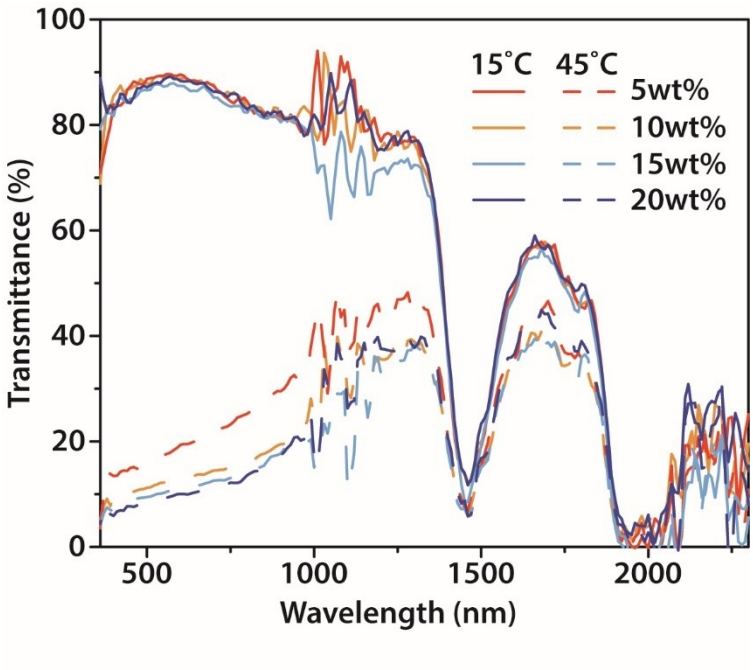

figure S1. UV-Vis spectra for smart hydrogels with different PNIPAm concentrations at 15 and 45 °C

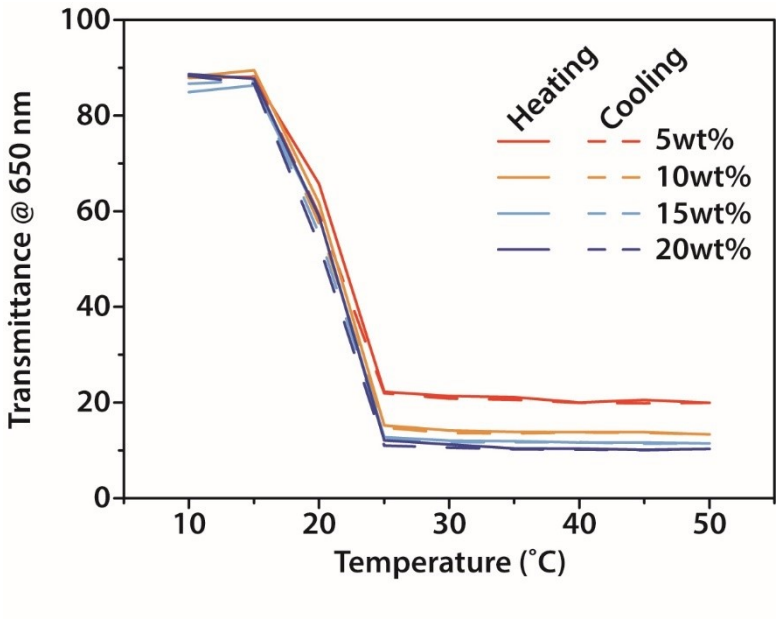

figure S2. Hysteresis loops for smart hydrogels with different PNIPAm concentrations.

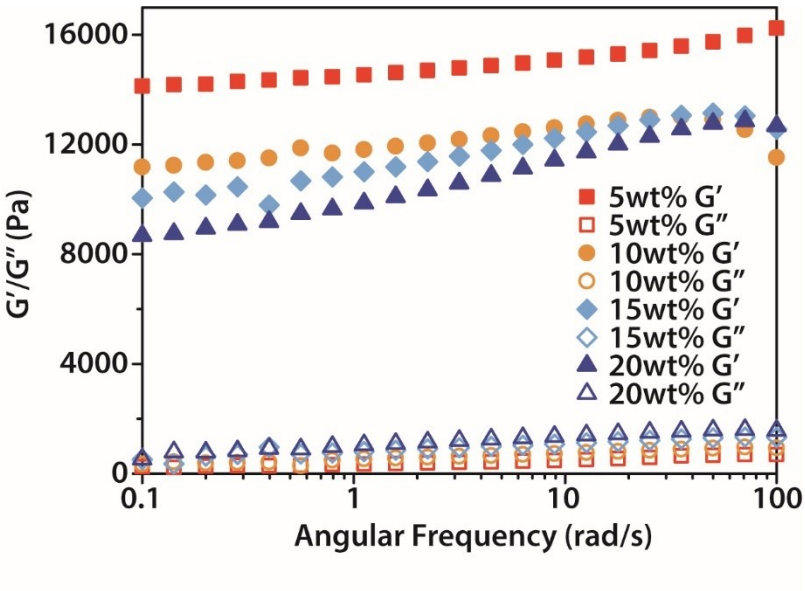

figure S3. G' and G" chart against angular frequency for the smart hydrogels with different PNIPAm concentrations.

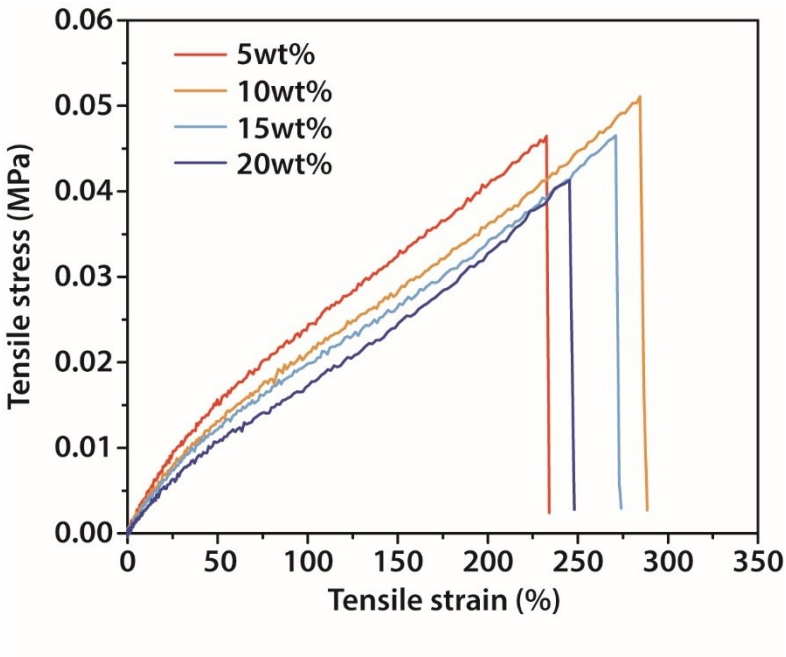

figure S4. Tensile curves for smart hydrogels with different PNIPAm concentrations.

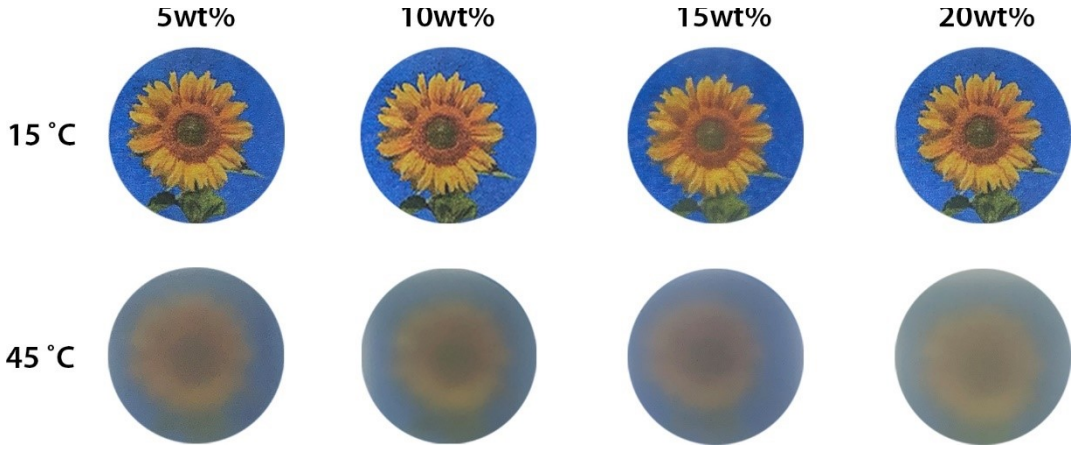

figure S5. Photos of smart hydrogels with different PNIPAm concentrations at 15 and 45 °C.

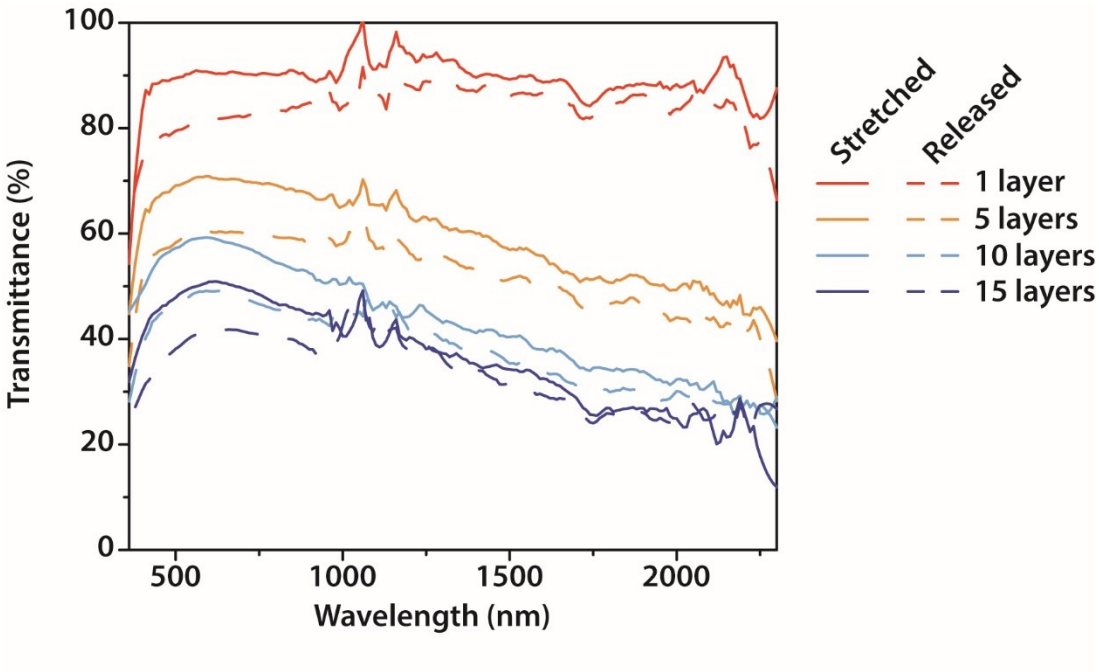

figure S6. UV-Vis spectra for different layers of AgNWs coated PDMS at stretched and released states.

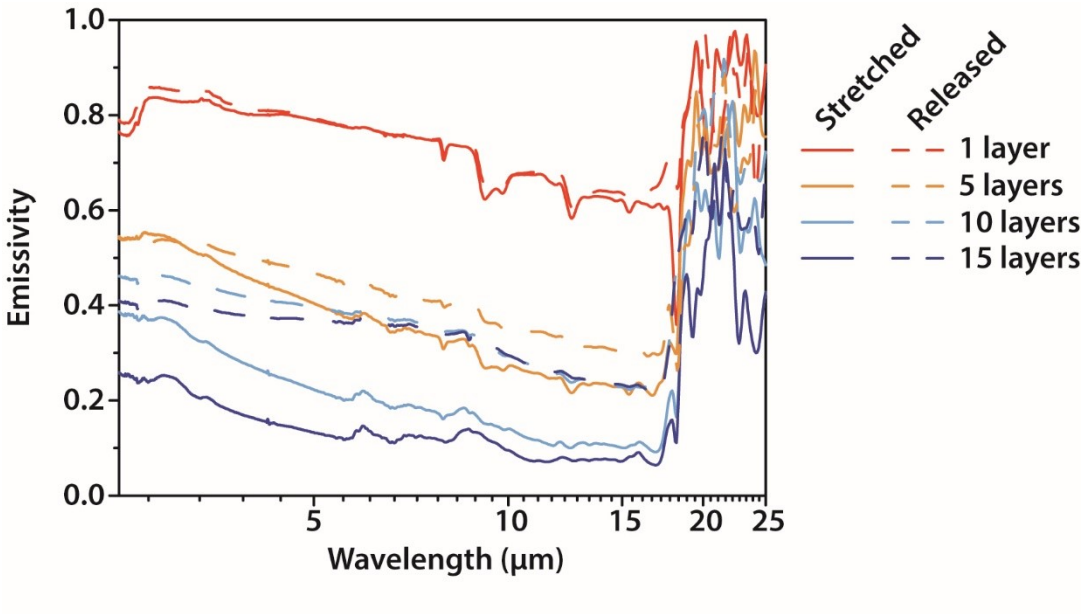

figure S7. Broadband emissivity spectra for different layers of AgNWs coated PDMS at stretched and released states.

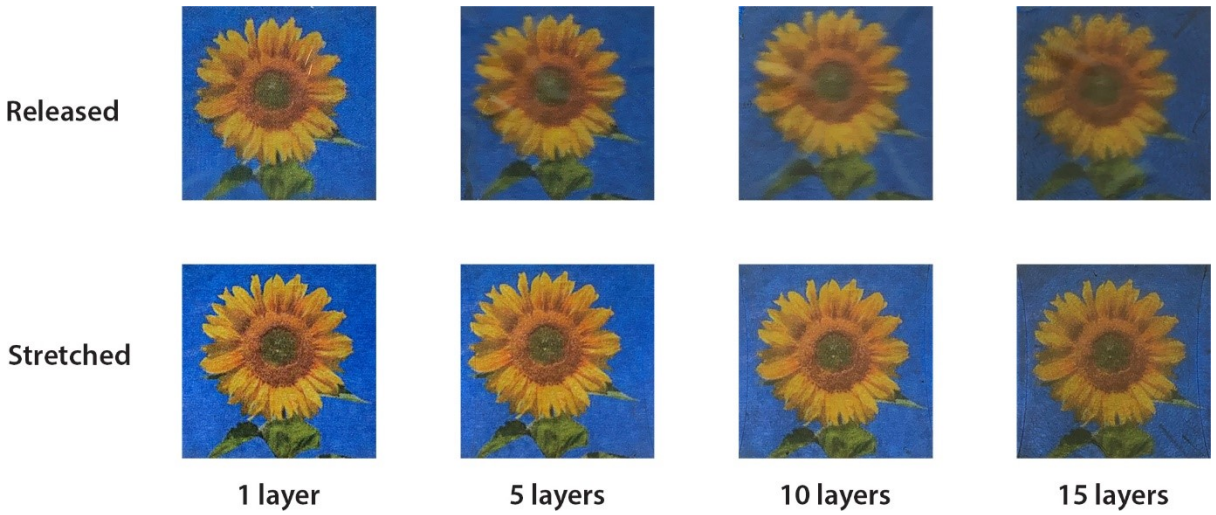

figure S8. Photos of different layers of AgNWs coated PDMS at stretched and released states.

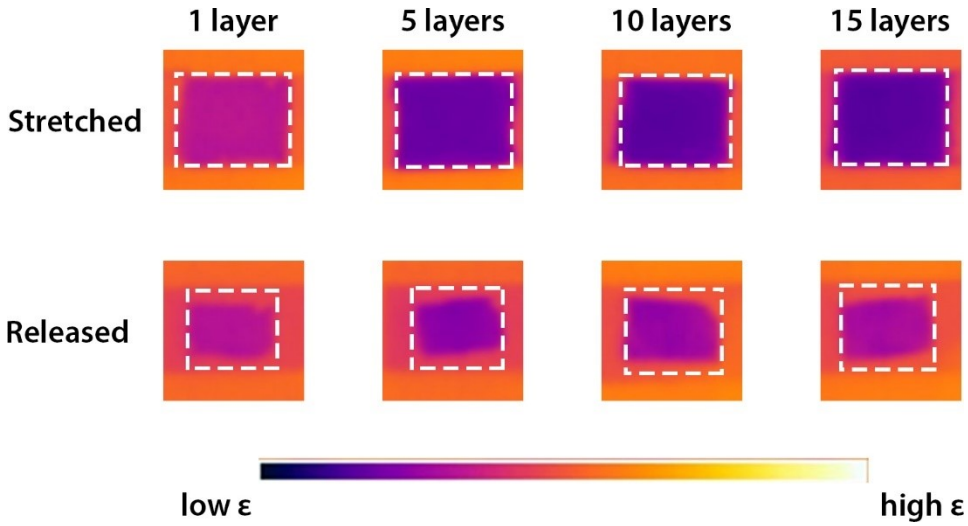

figure S9. IR camera images for different layers of AgNWs coated PDMS at stretched and released states. The samples are circled by dashed squares.

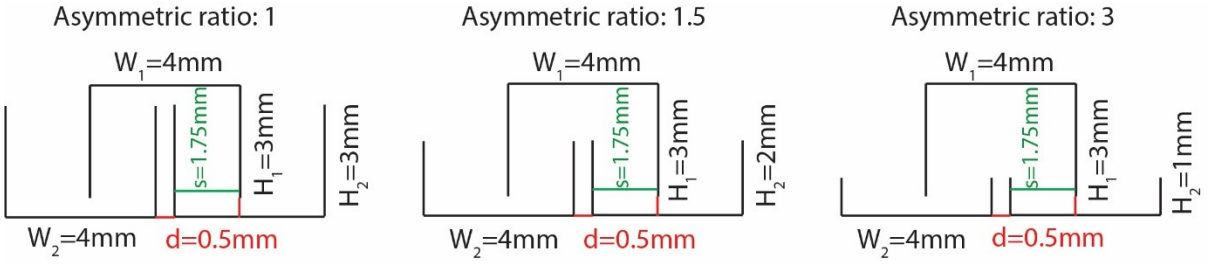

figure S10. Design of off-plain reconfigurable kirigami patterns with different geometric features.

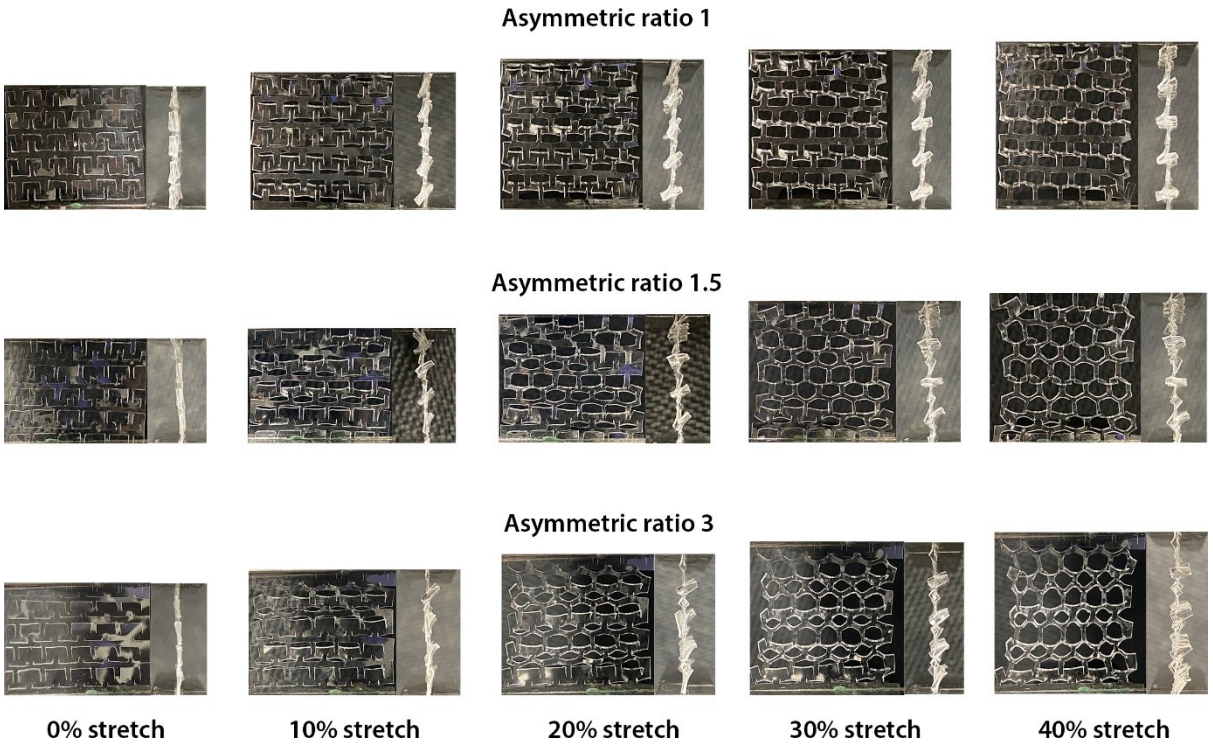

figure S11. Structure reconfiguration process for the kirigami structures with different asymmetric ratios.

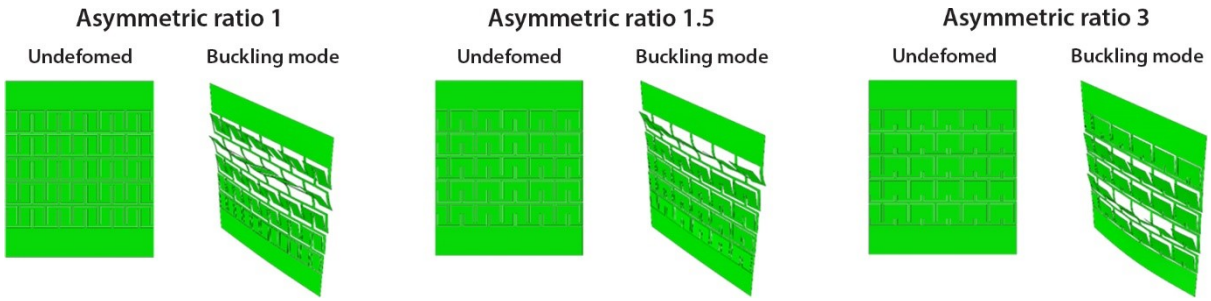

figure S12. FEM models of kirigami structures with different asymmetric ratios used for mechanical behaviour simulations.

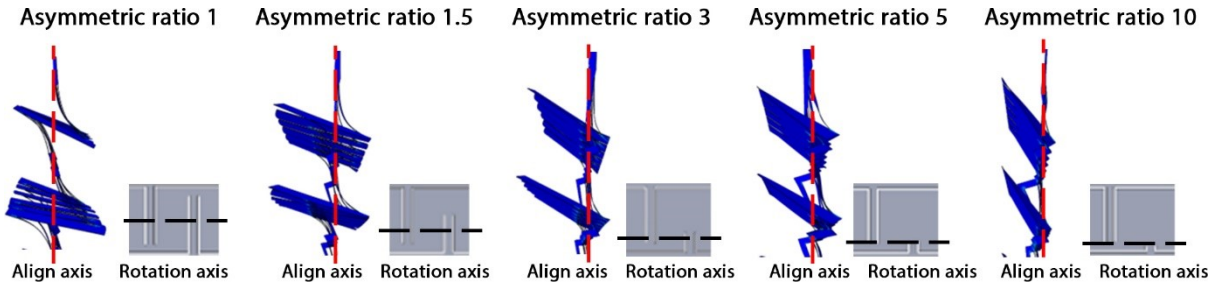

figure S13. Side views of the FEM simulated kirigami structures with different asymmetric ratios, their stretching direction, i.e., the aligning axis (red dashed line), and rotation axis (black dash line).

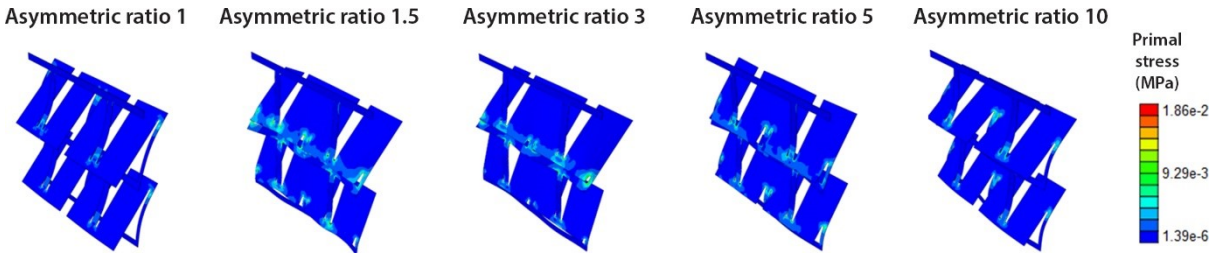

figure S14. Corner views of the primal stress distribution for the FEM simulated kirigami structures with different asymmetric ratios.

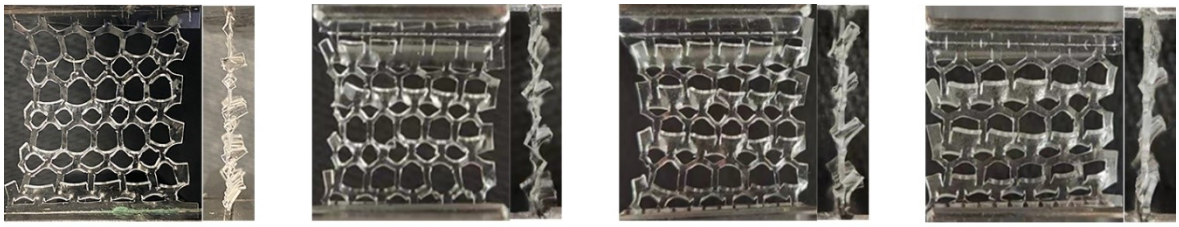

figure S15. Photos of out-of-plane kirigami structures with different PDMS thicknesses. The photos were taken with the 40% stretched samples.

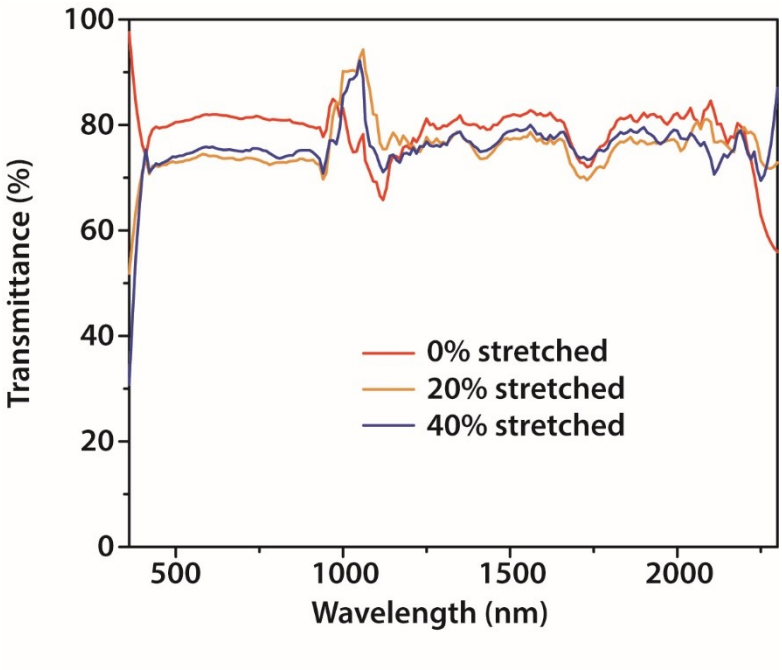

figure S16. UV-Vis spectra for the out-of-plane kirigami structure based on 0.3 mm PDMS under different strains.

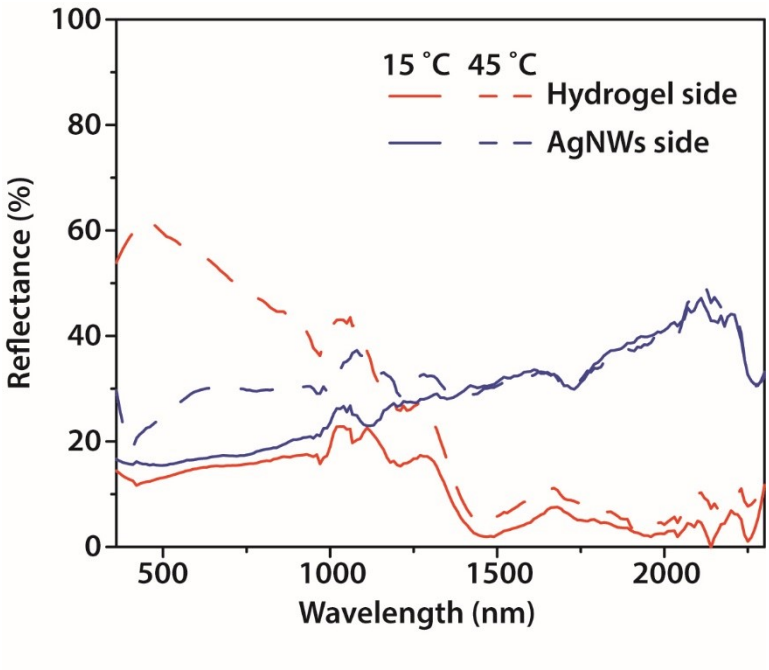

figure S17. Reflectance spectra for different sides of the durable solar/RC dual-control smart window at 15 and 45 °C.

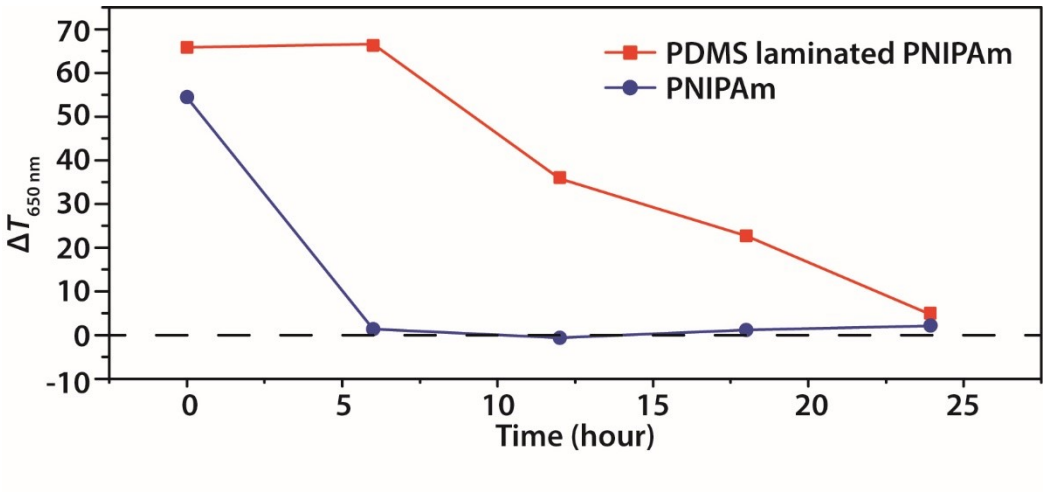

figure S18. High temperature (60 °C, 10%RH) durability test result for conventional PNIPAm and PDMS laminated PNIPAm.

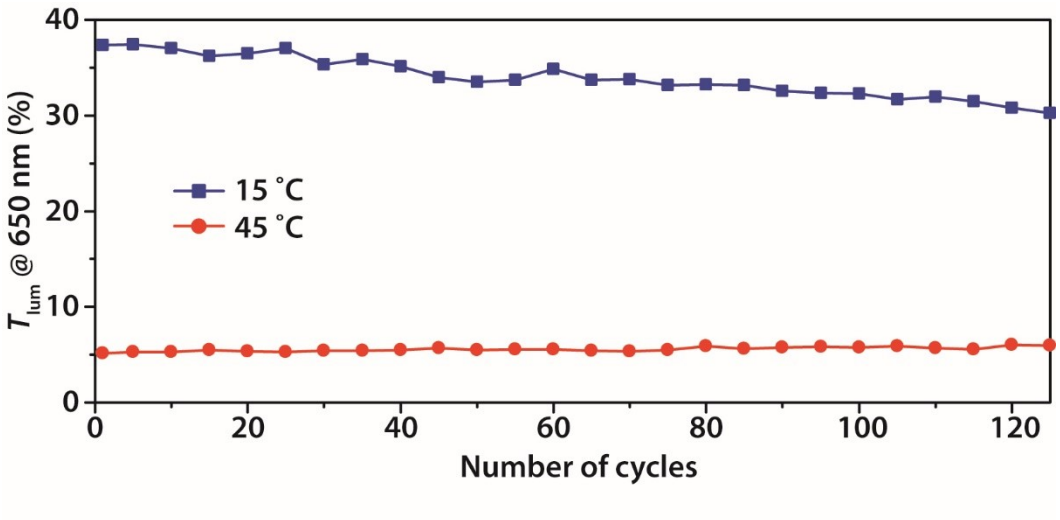

figure S19. Cycle stability for durable solar/RC dual-control smart window.

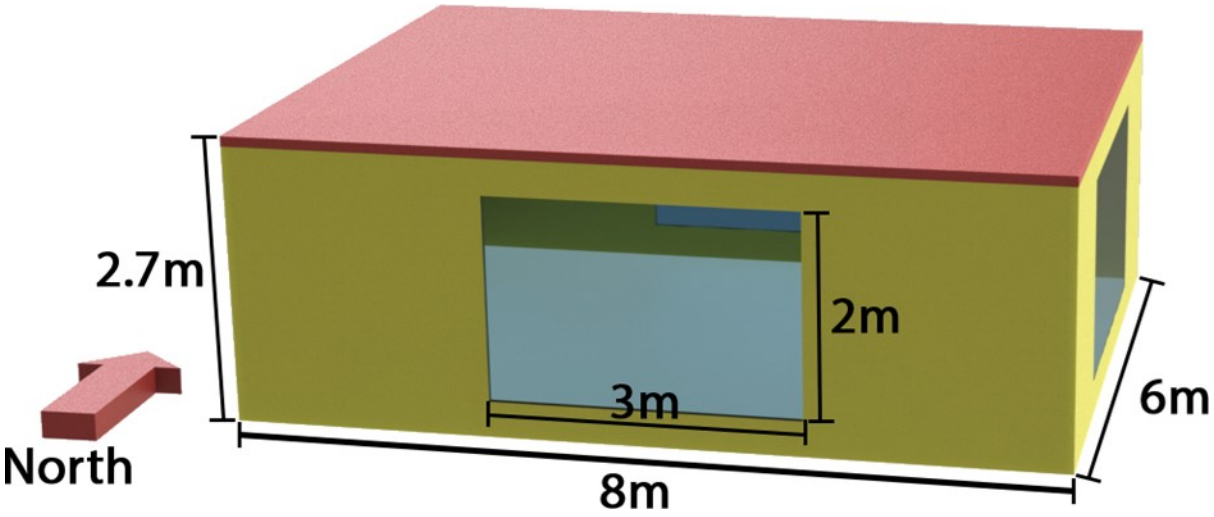

figure S20. Building model used for actual building energy consumption simulations and internal temperature simulations.

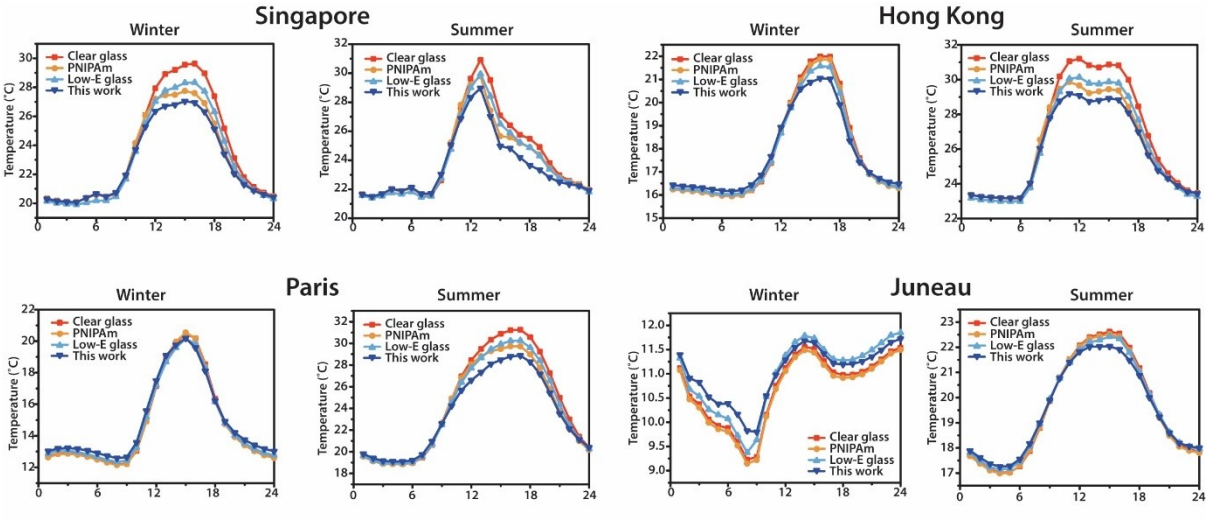

figure S21. 24-hour internal room temperature simulation results for clear glass, PNIPAm, low-E glass and durable solar/RC dual-control smart window in different climate regions and seasons. It should be noted that due to its tropical climate, there is no winter season in Singapore. Therefore, the room temperature curves for January and July are similar for Singapore.

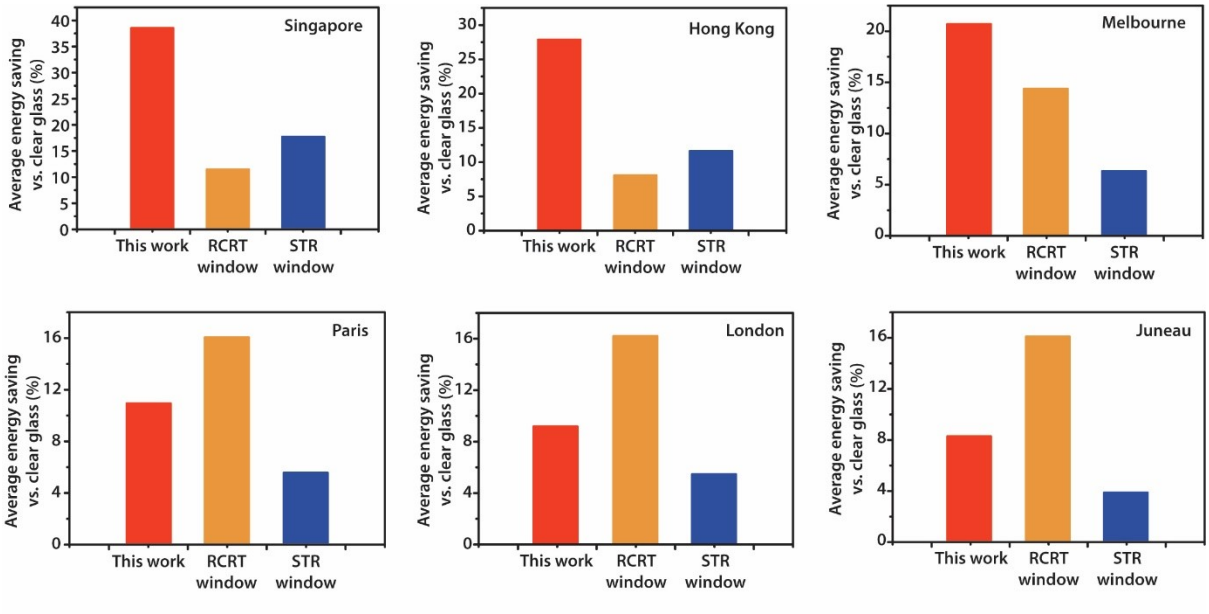

figure S22. Annual average energy saving performance for durable solar/RC dual-control smart window, RCRT smart window, and STR smart window in different cities. The clear glass was used as a baseline in this simulation.

table S1. Summary of optical properties for smart hydrogels and viscosities for monomer inks with different PNIPAm concentrations.

PNIPAm concentration	T_{lum} (%)	ΔT_{lum} (%)	ΔT_{sol} (%)	Viscosity (cP)
5wt%	89.2	76.6	54.1	115.8
10wt%	88.8	71.4	60.5	487.1
15wt%	87.3	76.9	60.3	1318.2
20wt%	88.3	79.0	62.3	2650.6

table S2. Summary of optical properties and Broadband emissivity for different layers of AgNWs coated PDMS.

AgNWs layer	T_{lum} (%)		T_{sol} (%)		$\varepsilon_{Broadband}$	
	Stretched	Released	Stretched	Released	Stretched	Released
1 layer	90.4	80.8	87.5	80.2	0.70	0.71
5 layers	70.2	59.8	64.5	55.7	0.36	0.42
10 layers	58.6	48.2	51.0	43.0	0.22	0.36
15 layers	49.8	43.3	40.5	37.2	0.16	0.34

table S3. Optical properties and Broadband emissivity for clear glass, PNIPAm hydrogel, commercial low-E glass, and durable solar/RC dual-control smart window used for energy simulation.

Simulation parameters	Clear glass	Conventional hydrogel	Commercial low-E glass	Durable solar/RC dual-control smart window
T_{lum} (%)	89.8	90.2 (20 °C) 5.5 (40 °C)	85	37.1 (15 °C) 6.7 (30 °C)
$R_{lum\text{-}Front}$ (%)	8.1	5.1 (20 °C) 26.9 (40 °C)	5.6	16.2 (15 °C) 27.7 (30 °C)
$R_{lum\text{-}Back}$(%)	8.1	5.1 (20 °C) 26.9 (40 °C)	7.9	14.2 (15 °C) 57.3 (30 °C)
T_{sol} (%)	83.7	66.8 (20 °C) 6.5 (40 °C)	63	30.6 (15 °C) 6.9 (30 °C)
$R_{sol\text{-}Front}$ (%)	7.5	5.9 (20 °C) 19.6 (40 °C)	19	19.8 (15 °C) 28.4 (30 °C)
$R_{sol\text{-}Back}$ (%)	7.5	5.9 (20 °C) 19.6 (40 °C)	22	14.1 (15 °C) 44.4 (30 °C)
$\varepsilon_{Broadband\text{-}Front}$	0.84	0.89	0.84	0.45 (15 °C) 0.95 (30 °C)
$\varepsilon_{Broadband\text{-}Back}$	0.84	0.89	0.1	0.95

video S1. FEM simulated structure reconfiguration animation for asymmetric ratio 1 kirigami structure.

video S2. FEM simulated structure reconfiguration animation for asymmetric ratio 1.5 kirigami structure.

video S3. FEM simulated structure reconfiguration animation for asymmetric ratio 3 kirigami structure.

video S4. FEM simulated structure reconfiguration animation for asymmetric ratio 5 kirigami structure.

video S5. FEM simulated structure reconfiguration animation for asymmetric ratio 10 kirigami structure.

Reference

1. G. Li, J. Chen, Z. Yan, S. Wang, Y. Ke, W. Luo, H. Ma, J. Guan and Y. Long, *Mater. Horiz.*, 2023, **10**, 2004-2012.
2. H. Hu, S. Wang, S. Wang, G. Liu, T. Cao and Y. Long, *Adv. Funct. Mater.*, 2019, **29**, 1902922.
3. Y. Feng, S. Wang, Y. Li, W. Ma, G. Zhang, M. Yang, H. Li, Y. Yang and Y. Long, *Adv. Funct. Mater.*, 2023, **33**, 2211027.
4. Y. Ke, Q. Zhang, T. Wang, S. Wang, N. Li, G. Lin, X. Liu, Z. Dai, J. Yan, J. Yin, S. Magdassi, D. Zhao and Y. Long, *Nano Energy*, 2020, **73**, 104785.
5. G. Wyszecki and W. S. Stiles, *Color Science: Concepts and Methods, Quantitative Data and Fomulae*, Wiley, New York, Second Edition edn., 2000.
6. ASTM, *ASTM G173 Standard tables of reference solar spectral irradiances: direct normal and hemispherical on a 37 tilted surface*, American Society for Testing and Materials, Philadelphia, PA, USA, 2012.
7. Y. Ke, Y. Li, L. Wu, S. Wang, R. Yang, J. Yin, G. Tan and Y. Long, *ACS Energy Letters*, 2022, **7**, 1758-1763.
8. ANSI/ASHRAE/IES, *Energy standard for building except low-rise residential buildings*, 2016.
9. S. Wang, T. Jiang, Y. Meng, R. Yang, G. Tan and Y. Long, *Science*, 2021, **374**, 1501-1504.
10. C. Lin, J. Hur, C. Y. H. Chao, G. Liu, S. Yao, W. Li and B. Huang, *Sci. Adv.*, 2022, **8**, eabn7359.